ACS OMEGA

Article

Cite This: ACS Omega 2018, 3, 16728−16734

http://pubs.acs.org/journal/acsodf

Unveiling the Structure of MoS_x Nanocrystals Produced upon Laser Fragmentation of MoS_2 Platelets

Konstantina Alexaki, Athanasia Kostopoulou,* Maria Sygletou, George Kenanakis, and Emmanuel Stratakis*

Institute of Electronic Structure and Laser Foundation for Research and Technology - Hellas, Heraklion, 71110 Crete, Greece

Supporting Information

ABSTRACT: Transition-metal dichalcogenide MoS_2 nanostructures have attracted tremendous attention due to their unique properties, which render them efficient nanoscale functional components for multiple applications ranging from sensors and biomedical probes to energy conversion and storage devices. However, despite the wide application range, the possibility to tune their size, shape, and composition is still a challenge. At the same time, the correlation of the structure with the optoelectronic properties is still unresolved. Here, we propose a new method to synthesize various morphologies of molybdenum sulfide nanocrystals, on the basis of ultrashort-pulsed laser fragmentation of MoS_2 platelets. Depending on the irradiation conditions, multiple MoS_x morphologies in the form of nanoribbons, nanospheres, and photoluminescent quantum dots are obtained. Besides the detailed structural analysis of the various crystals formed, the structure−property relation is investigated and discussed.

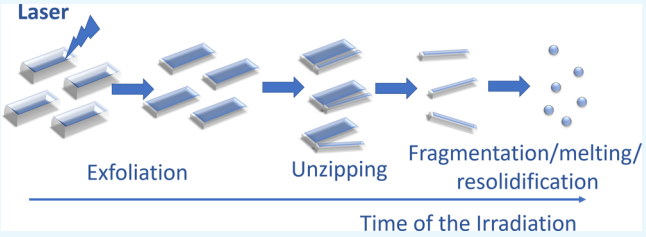

1. INTRODUCTION

Transition-metal dichalcogenides (TMDs) are unique two-dimensional (2D) materials due to their fascinating electronic, optical, and catalytic properties. The MoS_2, in particular, is a typical TMD comprising weakly bonded S−Mo−S sandwiched layers.[1] A single MoS_2 layer exhibits remarkably different properties than those of the bulk; the most pronounced one is that it is a direct-band gap semiconductor[2,3] contrary to the bulk, which shows an indirect band gap of 1.22 eV.[4] Their unique properties render them efficient nanoscale functional components for various applications, including sensors,[5] biomedicine,[6] and energy conversion and storage devices.[7,8]

Besides this, zero-dimensional (0D) TMDs have been found to exhibit high stability and extraordinary optoelectronic properties due to quantum confinement effects.[9−11] Such low-dimensional materials found numerous applications in electrochemical photocatalysis,[12,13] bioimaging,[14,15] and optoelectronic devices.[16] MoS_2 nanostructures, in particular, have been synthesized with different methods, such as ionic liquid-assisted grinding exfoliation,[12] hydrothermal routes,[10] electrochemical exfoliation,[17] colloidal methods at high temperature,[18] laser ablation in liquids,[19−26] and via an induced Fenton reaction.[27] Among them, the grinding exfoliation[12] and the hydrothermal[10] methods are time-consuming, considering that the first requires multiple centrifugation steps for the size selection of the particles whereas the second demands 18 h of reaction at 220 °C. Besides this, the electrochemical methods are two-step procedures and use hazardous materials.[17,27] Finally, the wet chemistry synthesis requires complex apparatus such as a Schlenk line and continuous inert gas flow during the reaction and takes place at high temperature, which increases the time and cost of the final products.[18]

The shape of the MoS_2 nanocrystals synthesized via the methods developed to date, is centrosymmetric, whereas the possibility to tune their size, shape, and composition is still a challenge. In this work, we propose a simple and rapid photoinduced method to control the morphology and stoichiometry of MoS_x nanostructures, via ultrashort-pulsed laser irradiation of MoS_2 platelets, in solution. It is a single-step, room temperature, and green process, providing different nanocrystal morphologies without the need of hazardous materials and additional surface functionalization. Besides this, it allows fundamental studies of the impact of crystal structure and morphology on the physicochemical properties of the MoS_x nanostructures. The rather simple and scalable method under ambient conditions provides unique opportunities for the cost-effective synthesis of bulk amounts of nanostructures with controllable size, shape, and stoichiometry.

2. RESULTS AND DISCUSSION

The initial colloidal solution of platelets has been prepared by laser ablation of a MoS_2 powder pellet in deionized water. For this purpose, a 513 nm laser source, emitting 170 fs pulses with a repetition rate of 60 kHz, has been used (Figure S1). The platelet colloids obtained by this process were stable in solution, and no precipitation was observed upon storage for months at ambient conditions. Subsequently, the aqueous

Received: June 19, 2018
Accepted: September 13, 2018
Published: December 5, 2018

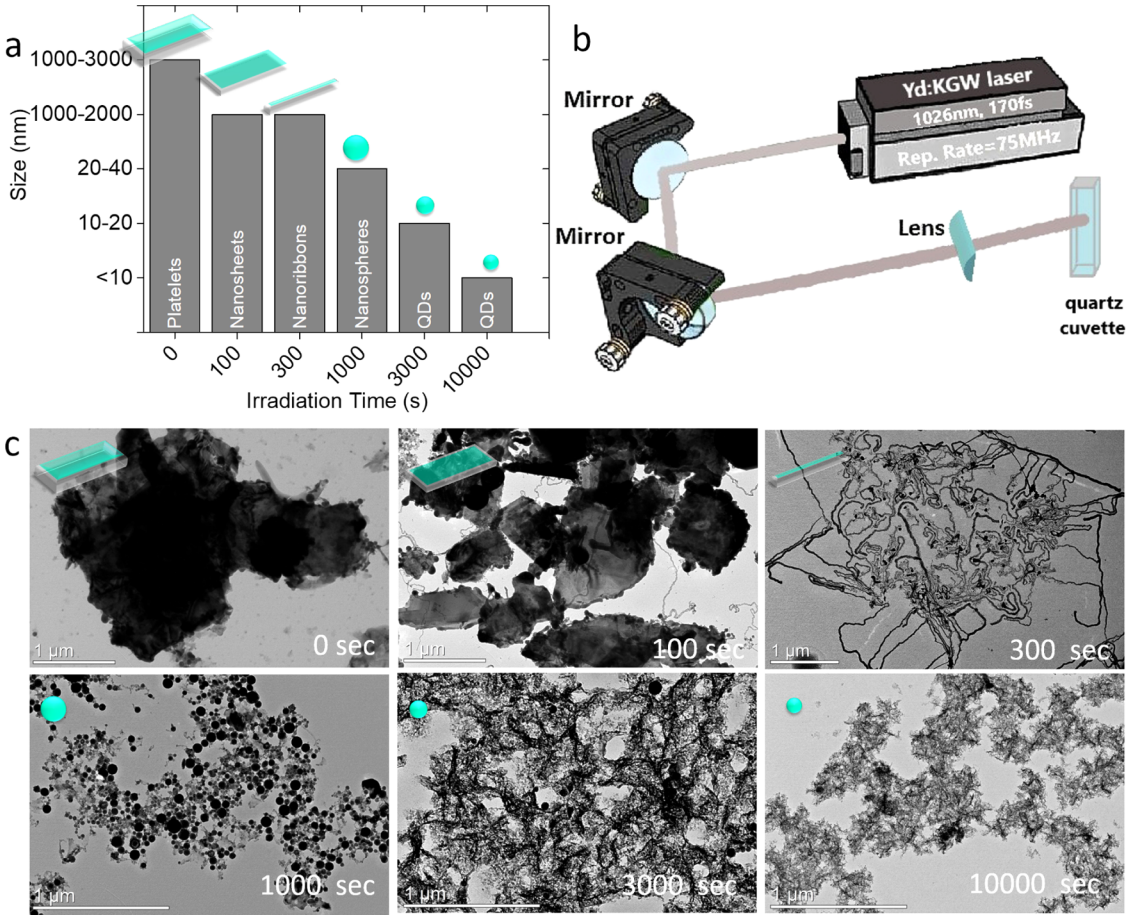

Figure 1. Size and shape evolution of the MoS_x structures by increasing the irradiation time of the platelet aqueous liquid (a). Schematic representation of the experimental setup utilized for the photoinduced fabrication of the nanostructures in liquid media under ambient conditions (b). Low-magnification transmission electron microscopy (TEM) images of the structures (c).

solution of MoS_2 platelets was irradiated using a 1030 nm laser source, emitting 170 fs pulses with a high repetition rate of 75 MHz (Figure 1b).

The influence of the irradiation time, ranging from 0 to 10 000 s, on the morphological and structural evolution of the of MoS_x nanostructures attained (Figure 1a) was carefully examined by TEM and Raman experiments. Representative, bright-field low-magnification TEM images for all structures obtained are presented in Figure 1c. In particular, the initial colloidal solution before the irradiation comprises bulk-like platelets, which have been ablated from the MoS_2 target. Following 100 s of irradiation, the as-prepared platelets become thinner (nanosheets), as indicated by the lighter contrast exhibited in the respective TEM images, while their lateral size becomes smaller. At 300 s of irradiation, nanoribbons of 20−50 nm width and length similar to that of the nanosheets prepared at 100 s are formed. Finally, above 1000 s of irradiation time, nanospheres are formed, with sizes down to 5 nm; the higher the exposure time, the lower is the mean nanosphere diameter produced.

Raman spectroscopy was used to probe the vibrational properties of the different structures formed. As shown in Figure 2, the two Raman peaks associated with $^1E_{2g}$ (in-plane motion of Mo and S in opposite directions) and A_{1g} (out-of-plane motions of S atoms) active modes are observed in all cases. In particular, for the nanosheets formed at 100 s, the two peaks are centered at 383.2 and 407.8 cm^{-1} (Table S1), in

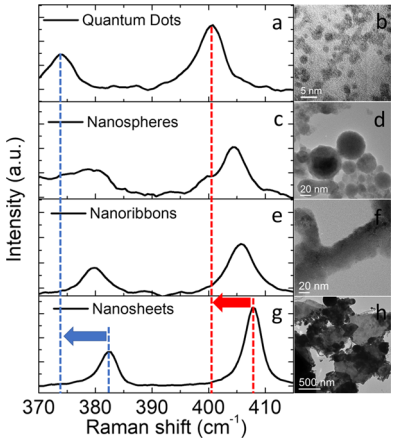

Figure 2. Raman spectra and TEM images: quantum dots obtained at 10 000 s of irradiation (a, b), nanospheres at 1000 s (c, d), nanoribbons at 300 s (e, f), and nanosheets at 100 s (g, h).

accordance to previous reports on bulk MoS_2.[28] Upon transition from nanosheets to nanoribbons and nanospheres, a characteristic blue shift and broadening of both peaks were observed. The blue shift is 3.4 cm^{-1} for the $^1E_{2g}$ and 2.1 cm^{-1} for the A_{1g} for the nanosheet-to-nanoribbon transition. According to the literature, the thinning of bulk MoS_2 to ultrathin nanosheets comprising three layers leads to a blue shift of the $^1E_{2g}$ and A_{1g} modes of about 0.6 and 2.1 cm^{-1},

DOI: 10.1021/acsomega.8b01390
ACS Omega 2018, 3, 16728−16734

respectively.[28] In addition, the broadening of these peaks has been associated with the decrease in the number of layers.[29] On the basis of these findings, the large blue shift of the $^1E_{2g}$ mode could not be solely attributed to the nanostructures thinning; therefore, another structural parameter could also play a role (Figure 3). No significant shift was observed, for

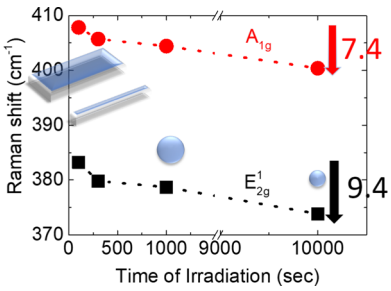

Figure 3. Peak position of the $^1E_{2g}$ and A_{1g} Raman modes, extracted by fitting the peaks in the Raman spectra with a Gaussian curve, for the different morphologies obtained ranging from platelets to quantum dots.

both modes, upon the transition from nanoribbons to nanospheres. However, the transformation of nanospheres to quantum dots gives rise to a further blue shift for both modes, namely, 4.9 for the $^1E_{2g}$ and 4 cm^{-1} for the A_{1g}, respectively. This observation is in contrast to the majority of literature results on Raman spectra of MoS_x nanostructures. For example, a red shift of the in-plane mode has been observed in monolayered structures of nanosheet[28] or quantum dot[30] morphologies. A large blue shift has been found only in the case of quantum dots prepared with an ionic liquid-assisted grinding exfoliation process, associated with disorder at the particles edges.[12] In addition, such large shift of the $^1E_{2g}$ mode (2.1 cm^{-1} per % strain) has been found in strained MoS_2 structures.[31] The shift is larger in the case of few-layered structures (2.1 cm^{-1} per % strain) compared with monolayered ones (1.7 cm^{-1} per % strain).

Furthermore, there are three different mechanisms that would explain the asymmetric broadening of the Raman peaks: (1) The broadening in the nanocrystalline materials is described by the phonon confinement model,[32] which leads to a breakup of selection rules, meaning, also, non-zone-center phonons will participate in scattering.[33−35] (2) The size/shape of the spectral lines is changing due to size effects of the grown nanostructures.[36] (3) The crystallinity of the material could affect the broadening of the peaks. A well-crystalline material yields a spectrum with very sharp, intense Raman peaks, whereas an amorphous material will show broader less intense Raman peaks. These two states (e.g., fully amorphous or fully crystalline) can be considered as spectral extremes, and a Raman spectrum from an intermediate state (e.g., partially crystalline) will have characteristics that are intermediate in terms of peak intensity and width (sharpness). On the basis of the Raman spectroscopy findings on disordered particles and strained layered structures and the three main mechanisms that could affect the broadening of the peaks stated above, we may postulate that apart from the reduction in the number of atomic layers, the laser-induced structural changes give rise to remarkable strain and disorder effects.

High-resolution transmission electron microscopy (HRTEM) analysis was used to evaluate the formation mechanism of the various kinds of nanostructures obtained. In particular, the following was observed.

2.1. For nanoribbons. HRTEM imaging revealed that the nanoribbons prepared upon 300 s of irradiation are crystalline (Figure 4) and have a width of w = 31.6 ± 11.1 nm (Figure

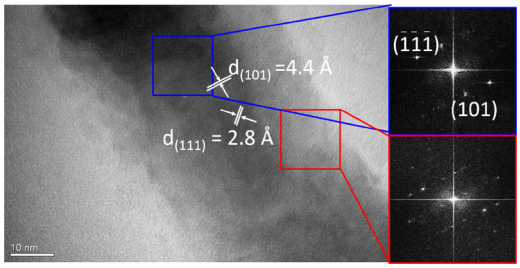

Figure 4. HRTEM image of an individual nanoribbon. The corresponding FFT patterns for the selected areas marked by rectangles in the middle (blue) and at the edge (red) of the nanoribbon are also presented. The zone axis in the image corresponds to the $[10\bar{1}]$ direction. The indexing has been assigned according to the reference pattern of the monoclinic Mo_2S_3 structure (ICSD, #073453).

S2a). The corresponding FFT patterns for the selected area, marked by a blue rectangle in the middle of the nanoribbons in Figure 4, cannot be indexed with the hexagonal structure of the MoS_2 (ICSD, #049801). The structure is compatible with the monoclinic structure of the Mo_2S_3 (ICSD, #073453), as the measured lattice spacings for the (111) and (101) are 2.8 and 4.4 Å, respectively. The corresponding Mo_2S_3 polymorph has been found in the literature to be formed due to surface phase transformation upon thermal annealing of MoS_2 at a temperature up to 1300 K[37] or by sputtering of MoS_2 films with low-energy Ar^+ ions[38]. Besides this, irradiation of MoS_2 monolayers with an electron beam leads to the introduction of sulfur vacancies.[39] Finally, the MoS_x phase was found in nanodots synthesized by the arc-melting method at 3000 °C, followed by a ball milling process.[40]

To further shed light on the structural features of the nanoribbons, we compared the FFT pattern calculated from an area in the middle to that at the edge of an individual nanoribbon (Figure 4). Although the central part is well-crystalline and there is no evidence for grain boundaries, the FFT pattern corresponding to the nanoribbon edge revealed the presence of disorder; the observed streaking in diffraction spots, in particular, indicates the existence of a stacking fault area along the b axis.

2.2. For nanospheres. Following 1000 s of laser irradiation, nanospheres of d = 36.2 ± 10.9 nm in diameter (Figure S2b) have been formed. HRTEM analysis revealed the presence of different types of particles. The majority are single-phase twined particles (Figure 5a), and a relatively small number of fullerene-like or amorphous particles (Figures 5b and S5) has been additionally observed. Fullerene particles have been synthesized by a similar laser-ablation technique in aqueous solution.[26,41] FFT pattern analysis revealed the crystal structure of the single-phase particles, which is compatible with the monoclinic structure of the Mo_2S_3 (ICSD, #073453). Indeed, lattice fringes with interplanar spacings of 3.0 and 2.2 Å have been identified, which are assigned to the (200) and (210) of the monoclinic crystal Mo_2S_3 structure, respectively. It should be noted here that the crystal structure of such nanocrystals is the same as that of the nanoribbons, although a

DOI: 10.1021/acsomega.8b01390
ACS Omega 2018, 3, 16728−16734

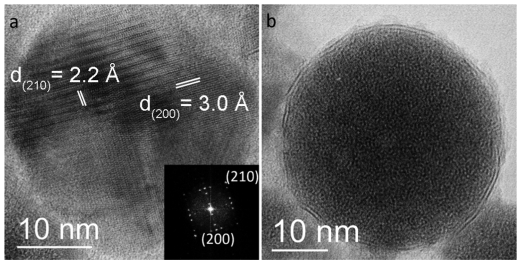

Figure 5. HRTEM images from the two different types of nanospheres, namely, single-phase twined (a) and fullerene-like (b) nanosphere. The inset in (a) is an FFT pattern corresponding to an individual nanosphere. The zone axis is the [001]. The indexing has been assigned according to the reference pattern of the monoclinic structure of the Mo_2S_3 (ICSD, #073453).

small percentage of nanoparticles exhibit the rhombohedral crystal symmetry of the Mo_3S_4 (Figure S3). The coexistence of these two phases in the same sample has been also found in previous reports.[40] The mixture of several molybdenum multisulfides has also been confirmed from the stoichiometry found by energy-dispersive spectrometry (EDS) analysis in different areas of the sample (Figure S4). This stoichiometry was found to be MoS (1:1), which is far away from the stoichiometry Mo/S = 1:2 of the MoS_2 target. Upon careful inspection of the HRTEM images and the corresponding FFT pattern, it can be concluded that the particles exhibit a quasispherical morphology of the twined type, revealed by the additional spots between the spots of the monoclinic phase. Variation of the Mo/S ratio in MoS_2 crystal structures has been found in the literature that it is associated with the presence of S vacancies.[42] Twin defects, dislocations, and grain boundaries in the crystal structure are accumulated by sulfur vacancies.[43,44] A ratio of 1.2 found in substoichiometric bilayers of MoS_2 due to lattice distortion originated from exfoliation process using hydrazine salts.[45]

2.3. For the quantum dots. Quantum dots with diameter d = 6.5 ± 1.6 nm (Figure S2c) are formed above 10 000 s of laser irradiation. Selected area diffraction analysis of a random area of the quantum dot sample (Figure S6) revealed the crystal structure of the quantum dots, which is compatible to the monoclinic crystal structure of Mo_2S_3 (Figure 6a). No indication for molybdenum oxide has been found due to possible oxidation of the surface.[46−48] This conclusion is in good agreement with the Raman spectra at the higher shift region. Peaks at 666 and 820 nm that could be assigned to the stretching modes of the triply coordinated oxygen (Mo_3−O) and the doubly coordinated oxygen (Mo_2−O) of the a-MoO_3 phase[49,50] are found only for the case of the nanospheres (Figure S7). The corresponding FFT pattern calculated from the HRTEM images (Figures 6b and S8) indicated a twined structure.

Notably, the quantum dots are photoluminescent at room temperature upon their excitation by a 248 nm laser beam (Figure 6c). In particular, a single PL peak is observed centered at 448 nm whereas no additional peaks are observed at longer wavelengths, indicating the absence of quantum dot aggregation. A similar spectrum has been recorded for the nanospheres (Figure S9). The main features are similar, but the spectrum of the nanospheres is blue-shifted compared to that of quantum dots. This is a contradictory result if we consider the particle size of the two samples. This is due to

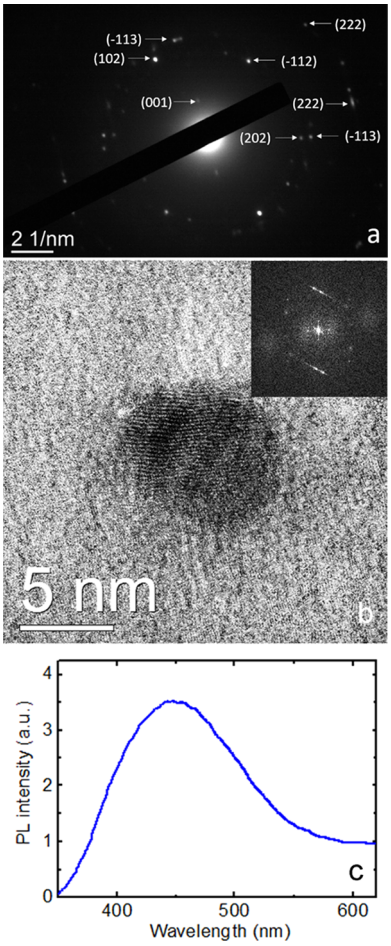

Figure 6. Selected area diffraction pattern (SAED) (a), HRTEM image (b), and photoluminescence spectrum (c) from the quantum dots formed above 10 000 s of laser irradiation. The inset in (b) is the corresponding FFT pattern calculated for an individual quantum dot (right). The indexing of the SAED has been assigned according to the reference pattern of the monoclinic structure of the Mo_2S_3 (ICSD, #073453).

existence of different particles (mainly of MoO_3) in the sample of the nanospheres.

Similar spectra have been recorded for water soluble 1,4-diaminobutane-functionalized MoS_2 quantum dots of about 5 nm synthesized by a bottom-up approach.[51]

On the basis of the above analysis, we may speculate on the formation mechanism that accounts for the structure and shape evolution of the various MoS_x nanostructures observed (Figure 7). Initially, laser irradiation of MoS_2 platelets gives rise to the photoinduced exfoliation to form few-layered nanosheets. The subsequent irradiation of nanosheets leads to the photo-induced unzipping[52−54] of the nanosheets' edges to form nanoribbons, which are crystalline in the Mo_2S_3 structure, exhibiting structural defects at their edges. This explanation complies with previous reports, where the Mo_2S_3 polymorph was found at the edges of MoS_2 nanosheets.[37] Upon further irradiation, the nanoribbons transform in nanospheres through a laser-induced melting and subsequent resolidification.[41,55] The temperature in the irradiated area due to the laser energy absorption is increased above the melting point of the material, and melted MoS_x droplets are formed. The resolidification occurs when the surface temperature of the droplets reduces below the melting point of MoS_x. The preferable shape of

DOI: 10.1021/acsomega.8b01390
ACS Omega 2018, 3, 16728−16734

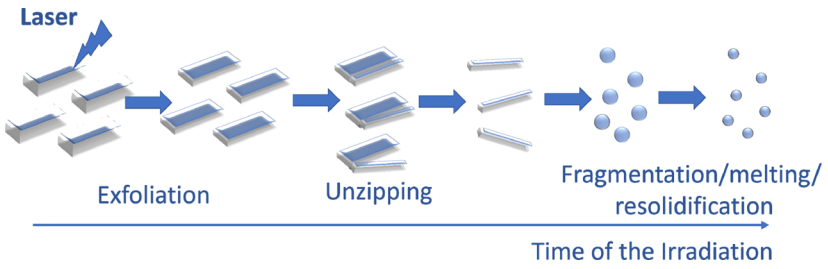

Figure 7. Photoinduced formation mechanism for the different MoS_x morphologies.

these structures tends to be spherical to reduce their surface energy. The observed strained structure of the nanoparticles revealed by HRTEM analysis could explain the large blue shift observed in the respective Raman modes. Finally, the nanoparticles break into smaller particles in the form of quantum dots, due to laser-induced ablative fragmentation of the larger nanospheres[56,57] indicated by the preservation of the initial Mo_2S_3 twined structure.

3. CONCLUSIONS

In summary, this work illustrates that laser irradiation of MoS_2 bulklike platelets could be used as an effective way for the synthesis of different morphologies of molybdenum multisulfides. This approach is simple, scalable, performed under ambient conditions, and can therefore be useful for the cost-effective synthesis of bulk amounts of nanostructures with controllable size, shape, and stoichiometry. More important, the various nanocrystal morphologies can be produced without the need of hazardous chemicals and additional surface functionalization processes, which make this technique appealing for many potential applications.

4. MATERIAL AND METHODS

4.1. Preparation of the Different Colloids. *4.1.1. Production of the Aqueous Solution of MoS_2 Platelets.* Initially, a MoS_2 target has been prepared via pressing MoS_2 powder into a pellet of 15 mm diameter. This target was placed at the bottom of a glass vial and immersed into 2 mL of deionized water. Subsequently, the beam of a Yb:KGW femtosecond laser was focused through the water layer, onto the target to exfoliate the MoS_2 powder into platelets (Figure S1). The laser wavelength, the repetition rate, the pulse duration, and the power used for this purpose were 513 nm, 60 kHz, 170 fs, and 90 mW, respectively. The total ablation time was 10 min. During laser irradiation, the target was continuously rotated using a rotation stage. All solutions obtained after irradiation were centrifuged at 1500 RPM for 10 min. Then, the supernatant colloidal solution is placed in a quartz cuvette for subsequent irradiation.

4.1.2. Synthesis of MoS_x Nanostructures (Figure 1). The as-prepared aqueous solution of the MoS_2 platelets was divided into 5 equivalent aliquots. Then, each aliquot was irradiated for 100, 300, 1000, 3000, and 10 000 s, respectively, using the same laser system, although at different irradiation parameters. In this case, the wavelength, repetition rate, pulse duration, and power used were 1026 nm, 75 MHz, 170 fs, and 4 mW, respectively. During the irradiation process, the colloidal solution was continuously agitated via use of a magnetic stirrer. The synthesis is reproducible, but the yield is low.

4.2. Characterization of the Colloidal Solutions. *4.2.1. Transmission Electron Microscopy (TEM).* Low-magnification and high-resolution TEM (HRTEM) images were recorded on a JEOL 2100 transmission electron microscope, operating at an accelerating voltage of 200 kV. For the purposes of the TEM analysis, a drop of the aqueous colloidal solution was deposited onto a carbon-coated copper TEM grid and then the solvent was allowed to evaporate. All images were recorded by a Gatan ORIUS SC 1000 CCD camera, whereas the structural features of the nanostructures were studied by two-dimensional (2D) fast Fourier transform (FFT) analysis.

4.2.2. Raman Spectroscopy. Raman measurements were performed at room temperature using a Horiba LabRAM HR Evolution confocal micro-spectrometer, in backscattering geometry (180°), equipped with an air-cooled solid-state laser operating at 532 nm, with 100 mW output power. The laser beam was focused on the samples using a 50× Olympus microscope objective (numerical aperture of 0.50), providing a ~22.5 mW power on each sample. Raman spectra over the 10−3000 cm^{-1} wavenumber range (with an exposure time of 20 s and 5 accumulations) were collected by a Peltier cooled CCD (1024 × 256 pixels) detector at −60 °C, with a resolution better than 1 cm^{-1} achieved thanks to an 1800 grooves/mm grating and an 800 mm focal length. Test measurements were carried out using different optical configurations, exposure time, beam power, and accumulations to obtain sufficiently informative spectra using a confocal hole of 100 μm but ensuring to avoid alteration of the sample, whereas the high spatial resolution allowed us to carefully verify the sample homogeneity. The wavelength scale was calibrated using a Silicon standard (520.7 cm^{-1}), and the acquired spectra were compared with scientific published data and reference databases, such as Horiba LabSpec 6 (Horiba).

4.2.3. Laser-Induced Fluorescence (LIF) Spectroscopy. Each solution was placed in quartz cuvette without further dilution, and the respective PL spectra were recorded at room temperature. For sample excitation, a KrF excimer laser, operating at 248 nm has been utilized. The pulse duration was about 20 ns, the excitation energy ~3.2 mJ, and the laser beam diameter 9.0 mm (fluence ~5 mJ/cm^2). The fluorescence measurements were performed at room temperature and recorded by a monochromator (PTI Technology) that is connected with an Andor iStar 734 Series Intensified Charge Coupled Device. The fluorescence signal of the samples was collected and guided to the spectrograph by an optical fiber.

4.2.4. Scanning Electron Microscopy (SEM) and Energy-Dispersive X-ray Spectroscopy (EDS). SEM (JEOL 7000), equipped with an EDS (INCA PentaFET-x3), was used for the analysis of the samples. These experiments were performed on solid-state samples produced after drying a small volume of the corresponding colloidal solution on a piece of a single-crystalline silicon wafer.

DOI: 10.1021/acsomega.8b01390
ACS Omega 2018, 3, 16728−16734

■ ASSOCIATED CONTENT

Supporting Information

The Supporting Information is available free of charge on the ACS Publications website at DOI: 10.1021/acsomega.8b01390.

EDS analysis, TEM images, size distributions, Raman spectra, PL curves and scheme of the setup for the laser ablation of the flakes in liquid media (PDF)

■ AUTHOR INFORMATION

Corresponding Authors

*E-mail: akosto@iesl.forth.gr (A.K.).
*E-mail: stratak@iesl.forth.gr (E.S.).

ORCID

Emmanuel Stratakis: 0000-0002-1908-8618

Author Contributions

The manuscript was written through contributions of all authors. All authors have given approval to the final version of the manuscript.

Funding

This work is supported by the European Research Infrastructure NFFA Europe, funded by EU's H2020 framework programme for research and innovation under grant agreement no. 654360.

Notes

The authors declare no competing financial interest.

■ ACKNOWLEDGMENTS

This work is supported by the European Research Infrastructure NFFA Europe, funded by EU's H2020 framework programme for research and innovation under grant agreement no. 654360. The support of Aleka Manousaki with SEM and EDS experiments is also acknowledged.

■ REFERENCES

(1) Eda, G.; Yamaguchi, H.; Voiry, D.; Fujita, T.; Chen, M. W.; Chhowalla, M. Photoluminescence from Chemically Exfoliated MoS2. *Nano Lett.* **2011**, *11*, 5111−5116.

(2) Mak, K. F.; Lee, C.; Hone, J.; Shan, J.; Heinz, T. F. Atomically Thin MoS2: A New Direct-Gap Semiconductor. *Phys. Rev. Lett.* **2010**, *105*, No. 136805.

(3) Bang, G. S.; Nam, K. W.; Kim, J. Y.; Shin, J.; Choi, J. W.; Choi, S. Y. Effective Liquid-Phase Exfoliation and Sodium Ion Battery Application of MoS2 Nanosheets. *ACS Appl. Mater. Interfaces* **2014**, *6*, 7084−7089.

(4) Roxlo, C. B.; Chianelli, R. R.; Deckman, H. W.; Ruppert, A. F.; Wong, P. P. Bulk and Surface Optical-Absorption in Molybdenum-Disulfide. *J. Vac. Sci. Technol., A* **1987**, *5*, 555−557.

(5) Huang, Y.; Guo, J. H.; Kang, Y. J.; Ai, Y.; Li, C. M. Two dimensional atomically thin MoS2 nanosheets and their sensing applications. *Nanoscale* **2015**, *7*, 19358−19376.

(6) Gu, Z.; Li, W. F.; Hong, L. B.; Zhou, R. H. Exploring biological effects of MoS2 nanosheets on native structures of alpha-helical peptides. *J. Chem. Phys.* **2016**, *144*, No. 175103.

(7) Zhu, C.; Mu, X. K.; van Aken, P. A.; Yu, Y.; Maier, J. Single-Layered Ultrasmall Nanoplates of MoS2 Embedded in Carbon Nanofibers with Excellent Electrochemical Performance for Lithium and Sodium Storage. *Angew. Chem., Int. Ed.* **2014**, *53*, 2152−2156.

(8) Tsai, M. L.; Su, S. H.; Chang, J. K.; Tsai, D. S.; Chen, C. H.; Wu, C. I.; Li, L. J.; Chen, L. J.; He, J. H. Monolayer MoS2 Heterojunction Solar Cells. *ACS Nano* **2014**, *8*, 8317−8322.

(9) Wilcoxon, J. P.; Samara, G. A. Strong Quantum-Size Effects in a Layered Semiconductor - Mos2 Nanoclusters. *Phys. Rev. B* **1995**, *51*, 7299−7302.

(10) Ren, X. P.; Pang, L. Q.; Zhang, Y. X.; Ren, X. D.; Fan, H. B.; Liu, S. Z. One-step hydrothermal synthesis of monolayer MoS2 quantum dots for highly efficient electrocatalytic hydrogen evolution. *J. Mater. Chem. A* **2015**, *3*, 10693−10697.

(11) Arul, N. S.; Nithya, V. D. Molybdenum disulfide quantum dots: synthesis and applications. *RSC Adv.* **2016**, *6*, 65670−65682.

(12) Benson, J.; Li, M. X.; Wang, S. B.; Wang, P.; Papakonstantinou, P. Electrocatalytic Hydrogen Evolution Reaction on Edges of a Few Layer Molybdenum Disulfide Nanodots. *ACS Appl. Mater. Interfaces* **2015**, *7*, 14113−14122.

(13) Lv, Z.; Mahmood, N.; Tahir, M.; Pan, L.; Zhang, X. W.; Zou, J. J. Fabrication of zero to three dimensional nanostructured molybdenum sulfides and their electrochemical and photocatalytic applications. *Nanoscale* **2016**, *8*, 18250−18269.

(14) Dai, W.; Dong, H. F.; Fugetsu, B.; Cao, Y.; Lu, H. T.; Ma, X. L.; Zhang, X. J. Tunable Fabrication of Molybdenum Disulfide Quantum Dots for Intracellular MicroRNA Detection and Multiphoton Bioimaging. *Small* **2015**, *11*, 4158−4164.

(15) Dong, H.; Tang, S. S.; Hao, Y. S.; Yu, H. Z.; Dai, W. H.; Zhao, G. F.; Cao, Y.; Lu, H. T.; Zhang, X. J.; Ju, H. X. Fluorescent MoS2 Quantum Dots: Ultrasonic Preparation, Up-Conversion and Down-Conversion Bioimaging, and Photodynamic Therapy. *ACS Appl. Mater. Interfaces* **2016**, *8*, 3107−3114.

(16) Mukherjee, S.; Maiti, R.; Katiyar, A. K.; Das, S.; Ray, S. K. Novel Colloidal MoS2 Quantum Dot Heterojunctions on Silicon Platforms for Multifunctional Optoelectronic Devices. *Sci. Rep.* **2016**, *6*, No. 29016.

(17) Gopalakrishnan, D.; Damien, D.; Li, B.; Gullappalli, H.; Pillai, V. K.; Ajayan, P. M.; Shaijumon, M. M. Electrochemical synthesis of luminescent MoS2 quantum dots. *Chem. Commun.* **2015**, *51*, 6293−6296.

(18) Yu, H.; Liu, Y.; Brock, S. L. Synthesis of discrete and dispersible MoS2 nanocrystals. *Inorg. Chem.* **2008**, *47*, 1428−1434.

(19) Sunitha, A. P.; Hajara, P.; Shaji, M.; Jayaraj, M. K.; Saji, K. J. Luminescent MoS2 quantum dots with reverse saturable absorption prepared by pulsed laser ablation. *J. Lumin.* **2018**, *203*, 313−321.

(20) Han, Q.; Cai, S. F.; Yang, L.; Wang, X. H.; Qi, C.; Yang, R.; Wang, C. Molybdenum Disulfide Nanoparticles as Multifunctional Inhibitors against Alzheimer's Disease. *ACS Appl. Mater. Interfaces* **2017**, *9*, 21116−21123.

(21) Hu, J. J.; Zabinski, J. S.; Bultman, J. E.; Sanders, J. H.; Voevodin, A. A. Encapsulated nanoparticles produced by pulsed laser ablation of MoS2-Te composite target. *Cryst. Growth Des.* **2008**, *8*, 2603−2605.

(22) Oztas, T.; Sen, H. S.; Durgun, E.; Ortac, B. Synthesis of Colloidal 2D/3D MoS2 Nanostructures by Pulsed Laser Ablation in an Organic Liquid Environment. *J. Phys. Chem. C* **2014**, *118*, 30120−30126.

(23) Ou, G.; Fan, P. X.; Ke, X. X.; Xu, Y. S.; Huang, K.; Wei, H. H.; Yu, W.; Zhang, H. J.; Zhong, M. L.; Wu, H.; Li, Y. D. Defective molybdenum sulfide quantum dots as highly active hydrogen evolution electrocatalysts. *Nano Res.* **2018**, *11*, 751−761.

(24) Ghobadi, A.; Ghobadi, T. G. U.; Okyay, A. K.; Ozbay, E. Emerging photoluminescence from defective vanadium diselenide nanosheets. *Photonics Res.* **2018**, *6*, 244−253.

(25) Wu, X.; Tian, X. M.; Chen, T. M.; Zeng, A.; Yang, G. W. Inorganic fullerene-like molybdenum selenide with good biocompatibility synthesized by laser ablation in liquids. *Nanotechnology* **2018**, *29*, No. 295604.

(26) Wu, H.; Yang, R.; Song, B. M.; Han, Q. S.; Li, J. Y.; Zhang, Y.; Fang, Y.; Tenne, R.; Wang, C. Biocompatible Inorganic Fullerene-Like Molybdenum Disulfide Nanoparticles Produced by Pulsed Laser Ablation in Water. *ACS Nano* **2011**, *5*, 1276−1281.

(27) Li, B. L.; Chen, L. X.; Zou, H. L.; Lei, J. L.; Luo, H. Q.; Li, N. B. Electrochemically induced Fenton reaction of few-layer MoS2

DOI: 10.1021/acsomega.8b01390
ACS Omega 2018, 3, 16728−16734

nanosheets: preparation of luminescent quantum dots via a transition of nanoporous morphology. *Nanoscale* **2014**, *6*, 9831−9838.
(28) Li, H.; Zhang, Q.; Yap, C. C. R.; Tay, B. K.; Edwin, T. H. T.; Olivier, A.; Baillargeat, D. From Bulk to Monolayer MoS2: Evolution of Raman Scattering. *Adv. Funct. Mater.* **2012**, *22*, 1385−1390.
(29) Gopalakrishnan, D.; Damien, D.; Shaijumon, M. M. MoS2 Quantum Dot-Interspersed Exfoliated MoS2 Nanosheets. *ACS Nano* **2014**, *8*, 5297−5303.
(30) Li, B.; Jiang, L.; Li, X.; Ran, P.; Zuo, P.; Wang, A. D.; Qu, L. T.; Zhao, Y.; Cheng, Z. H.; Lu, Y. F. Preparation of Monolayer MoS2 Quantum Dots using Temporally Shaped Femtosecond Laser Ablation of Bulk MoS2 Targets in Water. *Sci. Rep.* **2017**, *7*, No. 11182.
(31) Rice, C.; Young, R. J.; Zan, R.; Bangert, U.; Wolverson, D.; Georgiou, T.; Jalil, R.; Novoselov, K. S. Raman-scattering measurements and first-principles calculations of strain-induced phonon shifts in monolayer MoS2. *Phys. Rev. B* **2013**, *87*, No. 081307.
(32) Wolfrgang, D. *Laser Spectroscopy*, 4th ed.; Springer-Verlag Berlin: Heidelberg, 2008.
(33) Arora, A. K.; Rajalakshmi, M.; Ravindran, T. R.; Sivasubramanian, V. Raman spectroscopy of optical phonon confinement in nanostructured materials. *J. Raman Spectrosc.* **2007**, *38*, 604−617.
(34) Gouadec, G.; Colomban, P. Raman Spectroscopy of nanomaterials: How spectra relate to disorder, particle size and mechanical properties. *Prog. Cryst. Growth Charact. Mater.* **2007**, *53*, 1−56.
(35) Kumar, R.; Sahu, G.; Saxena, S. K.; Rai, H. M.; Sagdeo, P. R. Qualitative Evolution of Asymmetric Raman Line-Shape for NanoStructures. *Silicon* **2014**, *6*, 117−121.
(36) Campbell, I. H.; Fauchet, P. M. The Effects of Microcrystal Size and Shape on the One Phonon Raman-Spectra of Crystalline Semiconductors. *Solid State Commun.* **1986**, *58*, 739−741.
(37) Tiwari, R. K.; Yang, J. S.; Saeys, M.; Joachim, C. Surface reconstruction of MoS2 to Mo2S3. *Surf. Sci.* **2008**, *602*, 2628−2633.
(38) Ma, Q.; Odenthal, P. M.; Mann, J.; Le, D.; Wang, C. S.; Zhu, Y. M.; Chen, T. Y.; Sun, D. Z.; Yamaguchi, K.; Tran, T.; Wurch, M.; McKinley, J. L.; Wyrick, J.; Magnone, K.; Heinz, T. F.; Rahman, T. S.; Kawakami, R.; Bartels, L. Controlled argon beam-induced desulfurization of monolayer molybdenum disulfide. *J. Phys.: Condens. Matter* **2013**, *25*, No. 252201.
(39) Parkin, W. M.; Balan, A.; Liang, L. B.; Das, P. M.; Lamparski, M.; Naylor, C. H.; Rodriguez-Manzo, J. A.; Johnson, A. T. C.; Meunier, V.; Drndic, M. Raman Shifts in Electron-Irradiated Monolayer MoS2. *ACS Nano* **2016**, *10*, 4134−4142.
(40) Zhang, L. F.; Ou, G.; Gu, L.; Peng, Z. J.; Wang, L. N.; Wu, H. A highly active molybdenum multisulfide electrocatalyst for the hydrogen evolution reaction. *RSC Adv.* **2016**, *6*, 107158−107162.
(41) Zhou, L.; Zhang, H. W.; Bao, H. M.; Liu, G. Q.; Li, Y.; Cai, W. P. Onion-Structured Spherical MoS2 Nanoparticles Induced by Laser Ablation in Water and Liquid Droplets' Radial Solidification/Oriented Growth Mechanism. *J. Phys. Chem. C* **2017**, *121*, 23233−23239.
(42) Fabbri, F.; Rotunno, E.; Cinquanta, E.; Campi, D.; Bonnini, E.; Kaplan, D.; Lazzarini, L.; Bernasconi, M.; Ferrari, C.; Longo, M.; Nicotra, G.; Molle, A.; Swaminathan, V.; Salviati, G. Novel near-infrared emission from crystal defects in MoS2 multilayer flakes. *Nat. Commun.* **2016**, *7*, No. 13044.
(43) van der Zande, A. M.; Huang, P. Y.; Chenet, D. A.; Berkelbach, T. C.; You, Y. M.; Lee, G. H.; Heinz, T. F.; Reichman, D. R.; Muller, D. A.; Hone, J. C. Grains and grain boundaries in highly crystalline monolayer molybdenum disulphide. *Nat. Mater.* **2013**, *12*, 554−561.
(44) Lin, Z.; Carvalho, B. R.; Kahn, E.; Lv, R. T.; Rao, R.; Terrones, H.; Pimenta, M. A.; Terrones, M. Defect engineering of two-dimensional transition metal dichalcogenides. *2d Mater* **2016**, *3*, No. 022002.
(45) Daeneke, T.; Clark, R. M.; Carey, B. J.; Ou, J. Z.; Weber, B.; Fuhrer, M. S.; Bhaskaran, M.; Kalantar-zadeh, K. Reductive exfoliation of substoichiometric MoS2 bilayers using hydrazine salts. *Nanoscale* **2016**, *8*, 15252−15261.
(46) Cannon, P.; Norton, F. J. Reaction between Molybdenum Disulphide and Water. *Nature* **1964**, *203*, 750−751.
(47) Santosh, K. C.; Longo, R. C.; Wallace, R. M.; Cho, K. Surface oxidation energetics and kinetics on MoS2 monolayer. *J. Appl. Phys.* **2015**, *117*, No. 135301.
(48) Zhang, X.; Jia, F. F.; Yang, B. Q.; Song, S. X. Oxidation of Molybdenum Disulfide Sheet in Water under in Situ Atomic Force Microscopy Observation. *J. Phys. Chem. C* **2017**, *121*, 9938−9943.
(49) Lu, X. L.; Wang, R. G.; Hao, L. F.; Yang, F.; Jiao, W. C.; Zhang, J.; Peng, P.; Liu, W. B. Preparation of quantum dots from MoO3 nanosheets by UV irradiation and insight into morphology changes. *J. Mater. Chem. C* **2016**, *4*, 11449−11456.
(50) Ou, J. Z.; Carnpbell, J. L.; Yao, D.; Wlodarski, W.; Kalantar-zadeh, K. In Situ Raman Spectroscopy of H-2 Gas Interaction with Layered MoO3. *J. Phys. Chem. C* **2011**, *115*, 10757−10763.
(51) Haldar, D.; Dinda, D.; Saha, S. K. High selectivity in water soluble MoS2 quantum dots for sensing nitro explosives. *J. Mater. Chem. C* **2016**, *4*, 6321−6326.
(52) Vasu, K.; Yamijala, S. S. R. K. C.; Zak, A.; Gopalakrishnan, K.; Pati, S. K.; Rao, C. N. R. Clean WS2 and MoS2 Nanoribbons Generated by Laser-Induced Unzipping of the Nanotubes. *Small* **2015**, *11*, 3916−3920.
(53) Dimiev, A. M.; Khannanov, A.; Vakhitov, I.; Kiiamov, A.; Shukhina, K.; Tour, J. M. Revisiting the Mechanism of Oxidative Unzipping of Multiwall Carbon Nanotubes to Graphene Nanoribbons. *ACS Nano* **2018**, *12*, 3985−3993.
(54) Wei, D.; Xie, L.; Lee, K. K.; Hu, Z.; Tan, S.; Chen, W.; Sow, C. H.; Chen, K.; Liu, Y.; Wee, A. T. S. Controllable unzipping for intramolecular junctions of graphene nanoribbons and single-walled carbon nanotubes. *Nat. Commun.* **2013**, *4*, 1374.
(55) Yang, G. *Laser Ablation in Liquids: Principles and Applications in the Preparation of Nanomaterials*; Pan Stanford Publishing Pte. Ltd: Singapore, 2012.
(56) González-Rubio, G.; Guerrero-Martínez, A.; Liz-Marzán, L. M. Reshaping, Fragmentation, and Assembly of Gold Nanoparticles Assisted by Pulse Lasers. *Acc. Chem. Res.* **2016**, *49*, 678−686.
(57) Stratakis, E.; Barberoglou, M.; Fotakis, C.; Viau, G.; Garcia, C.; Shafeev, G. A. Generation of Al nanoparticles via ablation of bulk Al in liquids with short laser pulses. *Opt. Express* **2009**, *17*, 12650−12659.

DOI: 10.1021/acsomega.8b01390
ACS Omega 2018, 3, 16728−16734